WEARABLE TECHNOLOGY

Self-powered textile for wearable electronics by hybridizing fiber-shaped nanogenerators, solar cells, and supercapacitors

Zhen Wen,[1,2,3]* Min-Hsin Yeh,[1,4]* Hengyu Guo,[1,5]* Jie Wang,[1] Yunlong Zi,[1] Weidong Xu,[3] Jianan Deng,[1] Lei Zhu,[6] Xin Wang,[1] Chenguo Hu,[5] Liping Zhu,[2] Xuhui Sun,[3] Zhong Lin Wang[1,7]†

Wearable electronics fabricated on lightweight and flexible substrate are believed to have great potential for portable devices, but their applications are limited by the life span of their batteries. We propose a hybridized self-charging power textile system with the aim of simultaneously collecting outdoor sunshine and random body motion energies and then storing them in an energy storage unit. Both of the harvested energies can be easily converted into electricity by using fiber-shaped dye-sensitized solar cells (for solar energy) and fiber-shaped triboelectric nanogenerators (for random body motion energy) and then further stored as chemical energy in fiber-shaped supercapacitors. Because of the all–fiber-shaped structure of the entire system, our proposed hybridized self-charging textile system can be easily woven into electronic textiles to fabricate smart clothes to sustainably operate mobile or wearable electronics.

INTRODUCTION

Wearable electronics fabricated on lightweight and flexible substrate are widely believed to have great potential for portable devices (*1*–*3*). Several promising applications, for example e-skin, smartwatches, and bracelets, have been successfully achieved for the replacement of conventional electronic gadgets (*4*–*6*). Lightweight and wearable power supply modules with high energy storage performance are desirable for wearable technology. One strategy is to directly integrate a conventional rechargeable energy storage device, such as a battery or a supercapacitor (SC), into fabrics (*7*–*10*). This self-powered system is a favorable power platform to be integrated into wearable electronic systems. Fu *et al.* (*11*) designed a new type of integrated power fiber by incorporating a dye-sensitized solar cell (DSSC) and a solar cell for harvesting solar energy and storage to realize a self-powered system for driving a commercial light-emitting diode (LED). Du *et al.* (*12*) also proposed self-powered electronics by integration of flexible graphene-based SCs into perovskite hybrid solar cells. However, a photovoltaic cell works only under sufficient light illumination, and solar energy is not always available, strongly depending on the weather, working conditions, and so on. The intermittent and unpredictable nature of solar energy is an inevitable challenge for its expansion as a reliable power supply system in wearable electronics. The question of how to scavenge alternative energy from the environment with different types of energy harvesters, to compensate for the insufficient part of the solar energy, is urgent.

To develop a practical strategy to simultaneously scavenge multiple types of energies from the environment, the concept of a hybridized energy harvester incorporating two kinds of conversion cells for concurrently scavenging solar and mechanical energies was proposed, so that the energy resources could be effectively and complementarily used (*13*–*18*). Tribolectric nanogenerators (TENGs), are based on the coupling effect of contact electrification and electrostatic induction, and these have now been widely studied to harvest different mechanical energies from the environment (*19*–*23*). By using TENGs as the power supply, different types of self-powered systems were successfully demonstrated and realized, such as wireless sensors, chemical sensors, electrochemical reactions, home appliances, and security detection systems (*24*–*28*). Furthermore, to expand the practical applications of a TENG-based self-powered system, various structure types of flexible TENGs have been designed for harvesting ambient mechanical energy and, more adequately, for integration into wearable electronic devices (*29*–*31*). The high operating voltage of SCs can be directly achieved by charging them using a single TENG unit without additional in-series connection, which compensates for insufficient solar energy (*32*, *33*).

Here, we present a prototype of a fabric-hybridized self-charging power system not only for harvesting solar energy from ambient light but also for gathering mechanical energy from human motion. Both of the harvested energies can be easily converted into electricity by using fiber-shaped DSSCs (F-DSSCs) (for solar energy) and fiber-shaped TENGs (F-TENGs) (for mechanical energy) and then further stored as chemical energy in fiber-shaped SCs (F-SCs). Our proposed hybridized self-charging textile not only achieves reasonable energy conversion and storage capacity but also is inexpensive and can be easily fabricated. In addition, because of the all–fiber-based shape in each device, our proposed hybridized self-charging textile system can be easily woven into electronic textiles to fabricate smart clothes which operate wearable electronic devices.

RESULTS AND DISCUSSION

The double-layer structure of our proposed hybridized self-charging power textile is schematically illustrated in Fig. 1. Three kinds of

[1]School of Material Science and Engineering, Georgia Institute of Technology, Atlanta, GA 30332–0245, USA. [2]State Key Laboratory of Silicon Materials, School of Materials Science and Engineering, Cyrus Tang Center for Sensor Materials and Applications, Zhejiang University, Hangzhou 310027, China. [3]Jiangsu Key Laboratory for Carbon-Based Functional Materials and Devices, Institute of Functional Nano and Soft Materials, Soochow University, Suzhou, Jiangsu 215123, China. [4]Department of Chemical Engineering, National Taiwan University of Science and Technology, Taipei 10607, Taiwan. [5]Department of Applied Physics, Chongqing University, Chongqing 400044, China. [6]School of Material Science and Engineering, China University of Mining and Technology, Xuzhou, Jiangsu 221116, China. [7]Beijing Institute of Nanoenergy and Nanosystems, Chinese Academy of Sciences; National Center for Nanoscience and Technology, Beijing 100083, China.
*These authors contributed equally to this work.
†Corresponding author. Email: zhong.wang@mse.gatech.edu

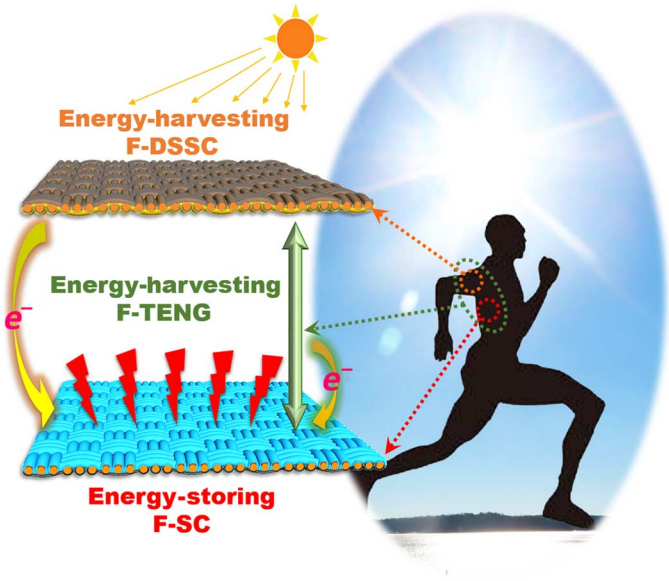

Fig. 1. Schematic of the self-charging power textile. Scheme of a fiber-based self-charging power system, which is made of an F-TENG, an F-DSSC as an energy-harvesting fabric, and an F-SC as an energy-storing fabric.

functional devices, including F-DSSCs, F-SCs, and F-TENGs, can be integrated spontaneously into a conventional textile structure. First, the top layer of the hybridized self-charging power textile is the F-DSSC–based textile, which is woven of several F-DSSC units for harvesting solar energy. Here, DSSC is chosen from numerous photovoltaic cells because DSSC materials and dyes can be tuned for optimization in a variety of lighting conditions, making it suitable for indoor and outdoor applications. Also, DSSCs can also be applied to a variety of substrates that are favorable for constructing the TENG structure. The F-SC–based textile acts as the bottom layer for storing the harvested energies. Meanwhile, each F-DSSC and F-SC unit is connected to one another, forming a single F-TENG unit; this F-TENG–based textile system is built to simultaneously scavenge body motion energy. Transparent and flexible ethylene vinyl acetate (EVA) tubing was used to build the basic unit of the self-charging power textile. Before the concurrent operation of the textile, the characterization of each functional device was carried out individually to evaluate its performance.

Initially, a single F-DSSC unit with a length of ~10 cm is constructed using N719 dye–sensitized TiO_2 nanotube arrays on a Ti wire as a working electrode and a Pt-coated carbon fiber as a counter electrode (CE), which is sealed into Cu-coated EVA tubing containing an I^-/I_3^--based electrolyte. Cu-coated EVA tubing acts not only as the holder for fabricating an F-DSSC but also as one electrode for F-TENG, which will be discussed later. The wire structure of the F-DSSC unit is schematically illustrated in detail in Fig. 2A. A photograph of a single F-DSSC unit is also presented in Fig. 2B. Figure 2C shows a low-magnification scanning electron microscopy (SEM) image of a Ti wire with a diameter of ~200 μm after anodic oxidation. A top-view high-magnification SEM image presented in Fig. 2D shows that the vertically oriented array of one-dimensional (1D) TiO_2 nanotubes is well grown on the Ti wire surface via electrochemical anodization, with a similar diameter of ~50 nm. Furthermore, the crystalline phases of the as-prepared TiO_2 nanotubes were examined by x-ray diffraction (XRD) patterns, as shown in fig. S1. Peaks corresponding to (101), (103), (004), (200), (105), and (211) of the TiO_2 anatase phase are observed (*34*). On the other hand, the SEM images of the Pt-coated carbon fiber and the bare carbon fiber are shown in fig. S2. It can be observed that the diameter of a single fiber (for both the Pt-coated carbon fiber and the pure carbon fiber) is ~10 μm. Homogeneous Pt nanoparticles were well dispersed on the surface of the carbon fiber, as a result of a thermally decomposed process. Afterward, the current-voltage (*I-V*) characteristic of a single F-DSSC unit was evaluated under standard illumination (100 mW cm^{-2}; AM1.5). Figure 2E shows the photocurrent density–voltage (*J-V*) curve of a single F-DSSC. The single F-DSSC unit exhibits a short-circuit current density (J_{SC}), an open-circuit voltage (V_{OC}), and a fill factor (FF) of 11.92 mA cm^{-2}, 0.74 V, and 0.64, respectively, corresponding to an overall power conversion efficiency of 5.64%. The dark current is also added in the figure as the reference. The performance of a single F-DSSC with bare carbon fibers is also examined for comparison, as shown in fig. S4. The performance of a single F-DSSC unit at different incident light angles is shown in fig. S5, and a detailed discussion can be found in the Supplementary Materials. A nonvolatile I^-/I_3^--based electrolyte was used in our study to enhance the long-term stability of the F-DSSC unit. The inset to Fig. 2E shows the electrochemical impedance spectra of a single F-DSSC unit for evaluating the charge transfer resistance in the device, which was measured under V_{OC} with an alternating current (ac) amplitude of 10 mV in the 100 kHz to 10 MHz frequency range. The ohmic series resistance (R_S) of a single F-DSSC unit can be determined in the high-frequency region of a Nyquist plot where the phase is zero. The first semicircle in the Nyquist plot at the high-frequency range corresponded to the impedance at the CE/electrolyte interface (R_{ct1}) for the reduction reaction of I_3^- ions, whereas the second semicircle at the middle frequency range corresponded to the charge-transfer impedance at the TiO_2/dye/electrolyte interface (R_{ct2}). The above results provide solid evidence that F-DSSCs had been successfully prepared for harvesting solar energy. To further apply F-DSSCs in our proposed self-charging power textile, the output performance of the F-DSSC at different bending angles should be considered. Figure 2F shows the normalized current density of a single F-DSSC at different bending degrees (from 0° to 180°) under a constant incident light intensity, where the value of the current density (~12 mA cm^{-2}) rarely changed under various bending angles, showing the stability of the photovoltaic device.

F-SCs are introduced in the self-charging power textile as the energy storage unit for F-DSSCs. A single F-SC unit with a length of 10 cm is symmetrically assembled with two carbon fibers coated with $RuO_2{\cdot}xH_2O$ in the H_3PO_4/PVA [poly(vinyl alcohol)] electrolyte and packaged into the polydimethylsiloxane (PDMS)–covered Cu-coated EVA tubing, as schematically shown in Fig. 3A. PDMS-covered Cu-coated EVA tubing acts not only as the holder for fabricating an F-SC but also as one electrode for F-TENG, which will be discussed later. Two bundles of carbon fibers were separated by a cellulose-based paper septum. A photograph of a single F-SC is shown in Fig. 3B. Here, long-ordered carbon fibers without any binders were directly used as the substrate for fabricating the F-SC owing to their excellent chemical stability and outstanding conductivity (*35*). $RuO_2{\cdot}xH_2O$ was synthesized on carbon fiber bundles by using a vapor-phase hydrothermal method to form binder-free fiber electrodes (*36*). A low-magnification SEM image of the as-synthesized $RuO_2{\cdot}xH_2O$–coated carbon fibers reveals that several carbon fibers were assembled into a bundle, as shown in Fig. 3C. Figure 3D shows a high-magnification SEM image of $RuO_2{\cdot}xH_2O$ coated on a single carbon fiber with a

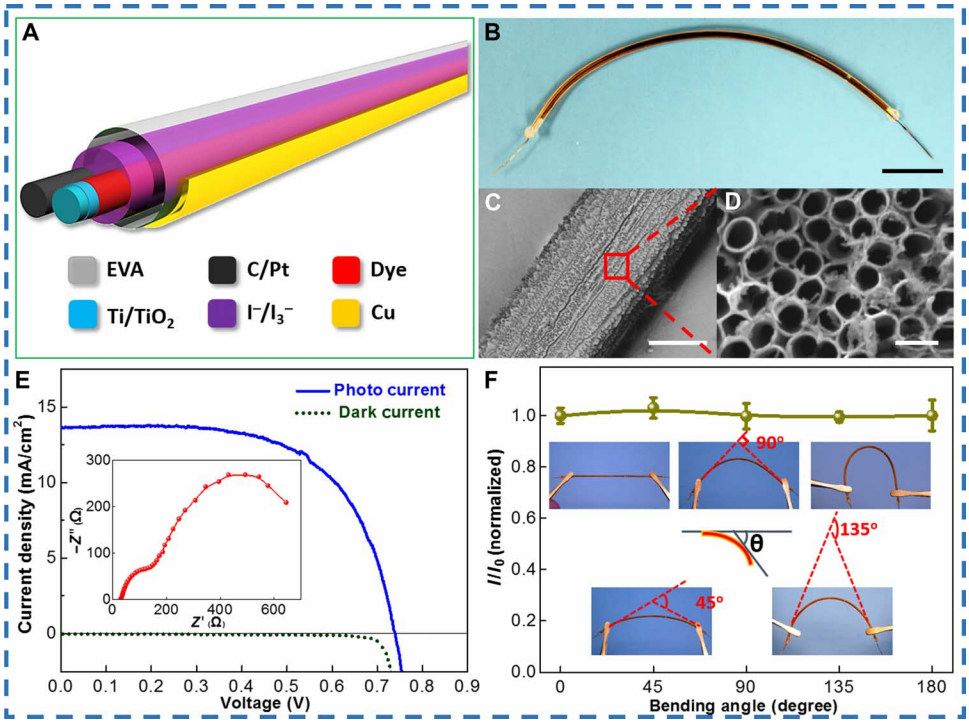

Fig. 2. Structural design of an F-DSSC. (**A**) Schematic diagram and (**B**) photograph (scale bar, 1 cm) of a single F-DSSC, consisting of N719 dye–adsorbed TiO_2 nanotube arrays on a Ti wire as a working electrode and a Pt-coated carbon fiber as a CE in an I^-/I_3^--based electrolyte. (**C**) Low-magnification and (**D**) high-magnification SEM images of the TiO_2 nanotube arrays on the Ti wire [scale bars, 100 μm (C) and 100 nm (D)]. (**E**) *J-V* curve of a single F-DSSC (inset shows the Nyquist plot of an F-DSSC, which is measured under V_{OC} with frequencies ranging from 100 kHz to 10 MHz). (**F**) Normalized current density of the single F-DSSC at different bending angles (0° to 180°) (insets show the photograph of a single F-DSSC at different bending angles).

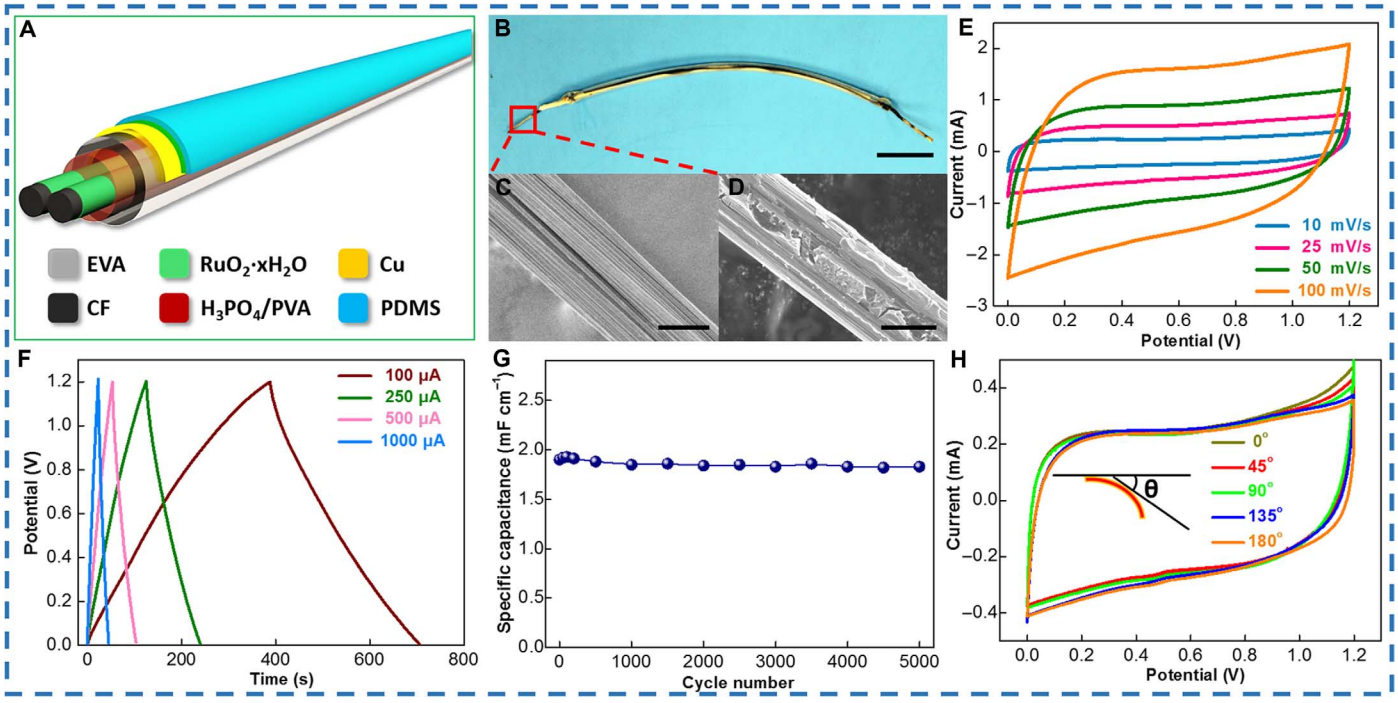

Fig. 3. Structural design of an F-SC. (**A**) Schematic diagram and (**B**) photograph (scale bar, 1 cm) of a single F-SC, consisting of two carbon fibers coated with $RuO_2{\cdot}xH_2O$ in the H_3PO_4/PVA electrolyte. (**C**) Low-magnification and (**D**) high-magnification SEM images of the $RuO_2{\cdot}xH_2O$–coated carbon fiber electrode [scale bars, 100 μm (C) and 5 μm (D)]. (**E**) CV of the single F-SC at different scanning rates (10 to 100 mV/s). (**F**) GCD curve of a single F-SC at different current densities (100 to 1000 μA). (**G**) Cycling performance of a single F-SC unit. (**H**) CV curves of the single F-SC at different bending angles (0° to 180°).

diameter of ~10 μm; it presents the typical "cracked mud" morphology on the surface of carbon fibers. Moreover, the crystalline phase of the as-synthesized fibers is confirmed by XRD patterns (fig. S5), and the peaks for each XRD pattern can be assigned to a typical amorphous $RuO_2{\cdot}xH_2O$ with a partly rutile crystalline structure, which is an essential phase to simultaneously obtain high ion and high electron conductivity (*37*). The electrochemical capacitance properties of a single F-SC unit were further evaluated by cyclic voltammetry (CV) and galvanostatic charging/discharging (GCD) techniques. To evaluate the fast charge/discharge ability of the F-SC, we examined CV at different scan rates (from 10 to 100 mV s^{-1}), as shown in Fig. 3E. It can be observed that the CV curves do not distort significantly as the scan rate increases, indicating their good capacitive behavior and high-rate capability. Figure 3F shows the charge/discharge curves of the F-SC at different current densities (from 100 to 1000 μA), with the potential ranging from 0 to 1.2 V. The symmetrically triangle-shaped GCD curves of the F-SC under various current densities can be observed. Moreover, no obvious *IR*-drop phenomenon can be found even at a short discharging time of 23 s, which reconfirms the outstanding capacitance behavior and the promising charging/discharging performance of the F-SC. As a comparison, the energy storage performances of the carbon fiber without incorporating RuO_2 were also measured, as shown in fig. S6. Because the mass-specific capacitance (F g^{-1}) is not suitable for F-SC, the length-specific capacitance (F cm^{-1}) was evaluated and then calculated in this study. Our results reveal that the specific capacitance of 1.9 mF cm^{-1} can still be retained at a high level under a high current density of 1000 μA, and its energy density is up to 1.37 mJ cm^{-1}, both of which demonstrate a fast charging/discharging ability and a reasonable energy density. The cycling stability of SC is also a critical issue that should be considered. The cycling performance of a single F-SC unit was investigated, as shown in Fig. 3G. No obvious capacitance change can be observed after 5000 cycles at a charging/discharging current of 1000 μA. The PVA/H_3PO_4 gel electrolyte has also demonstrated excellent cycling stability in our previous work (*34*). Finally, the capacitance of a single F-SC at different bending angles (from 0° to 180°) was also examined, as shown in Fig. 3H. All of the CV curves for a single F-SC unit with various bending angles exhibit typical and almost overlapping rectangle-like curves, indicating that it is a reliable platform for storing harvested energies with excellent flexibility and promising stability under various bending conditions.

As mentioned before, a pair of single F-TENG units can be built by pairing the F-DSSC with Cu-coated EVA tubing and the F-SC with PDMS-covered Cu-coated EVA tubing. A schematic diagram and a digital photograph of a pair of single F-TENG units are shown in Fig. 4 (A and B, respectively). To elucidate the working mechanism in a simplified model, the relative motion of the two fiber tubes can be simplified as the contact-separation process that occurs between Cu and PDMS, as illustrated in Fig. 4C. In the original state (i), the PDMS surface was charged with negative electrostatic charges and the Cu_1 electrode produced positive charges, due to the electrostatic induction and conservation of charges. When the F-TENG was pressed (ii), a shrinkage of the gap between the Cu_2 electrode and PDMS would result in induced positive charges accumulating in the Cu_2 layer because of the electrostatic induction. Accordingly, free electrons in Cu_2 would flow to the Cu_1 layer to balance the field. This

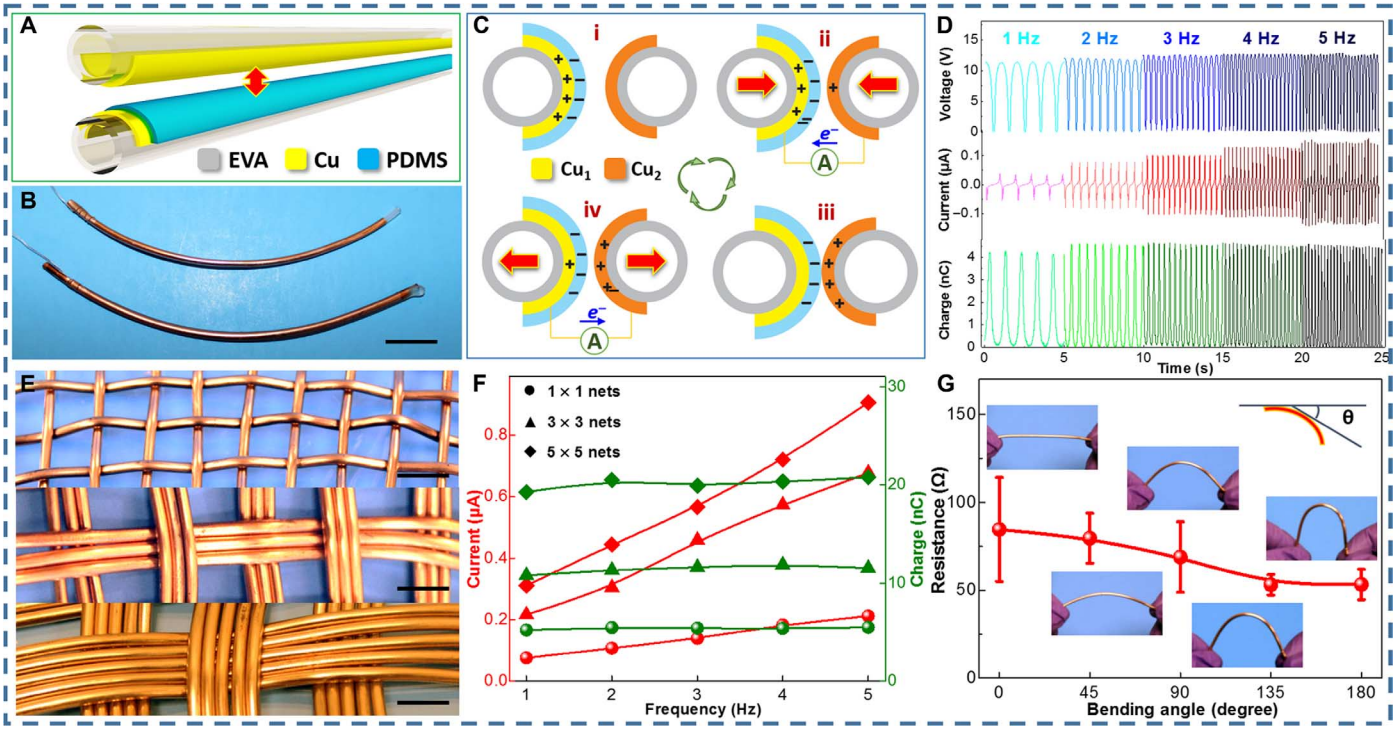

Fig. 4. Structural design of an F-TENG. (**A**) Schematic diagram and (**B**) photograph (scale bar, 1 cm) of a pair of single F-TENG units, consisting of a Cu-coated EVA tube and a PDMS-covered Cu-coated EVA tube. (**C**) Schematic illustration of the working mechanism of the F-TENG under parallel contact-separation motion. (**D**) Electrical outputs of a pair of F-TENG units, which included V_{OC}, I_{SC}, and Q_{SC}, at various motion frequencies (1 to 5 Hz). (**E**) Photograph of the wearable self-charging powered textile with knitting patterns of 1 × 1, 3 × 3, and 5 × 5 nets (all scale bars, 1 cm). (**F**) Triboelectric output performance of the three network textiles. (**G**) The electric resistance of the Cu-coated EVA tube at different bending angles (0° to 180°) (insets show the photograph of the Cu-coated EVA tube at different bending angles).

process produces an instantaneous positive current. It is necessary to note that the charges on PDMS will not be annihilated even when it makes contact with the Cu_2 electrode (iii), because the electrostatic charges are naturally impregnated into the insulator PDMS. In the reverse case, when the F-TENG was released (iv), it would recover back to its original state (i) and the internal gap would be increased. Thus, an instantaneous negative current could be produced. Therefore, a contact-separation process of the F-TENG will generate an ac through the load (*38*–*41*). The output performance of power generation for a pair of single F-TENG units with a length of ~10 cm was systematically studied via the periodic motion of contacting and separating under controlled frequencies. To analyze the output capability of the F-TENG, we used a linear motor to trigger the pair of single F-TENG units, wherein the maximum distance between the two tubing systems was purposely set at 10 mm. As shown in Fig. 4D, when motion frequencies vary from 1 to 5 Hz, the V_{OC} and transferred charges (Q_{SC}) remain constant (~12.6 V and ~4.5 nC, respectively). The short-circuit current (I_{SC}) increases from ~0.06 to ~0.15 μA, revealing a clear increasing trend with the increase in frequency. In other words, the increase in frequency is favorable for the magnitude of I_{SC}. Furthermore, three kinds of F-TENG–based textile with knitting patterns of 1 × 1, 3 × 3, and 5 × 5 nets are fabricated and then characterized under various motion frequencies (1 to 5 Hz), as shown in Fig. 4 (E and F, respectively). It indicates that the values of Q_{SC} and I_{SC} at 5 Hz increase with the increase in braided density from 1 × 1 nets (5.4 nC and 0.21 μA) to 3 × 3 nets (11.6 nC and 0.68 μA) and 5 × 5 nets (20.8 nC and 0.91 μA), as a result of the further enlargement of its conductive surface area for electrostatic induction. The V_{OC} remains almost constant because of the unchanged motion distance, as shown in fig. S7. As for wearable energy-harvesting textiles, the capability of F-TENG to withstand harsh bending or deformation is an essential requirement. Therefore, a flexibility test was performed, as shown in Fig. 4E and movie S1. No apparent change in resistance could be observed when a single Cu-coated EVA tubing was bent at different angles (from 0° to 180°). The photograph of the Cu-coated EVA at different bending angles is also shown as insets.

To construct the hybridized self-charging power textile, several F-DSSC and F-SC units were woven into an individual fabric as the textile structure with in-series/parallel connection. An F-TENG–based textile system can be built after connecting both textiles. Figure 5 (A to C) shows a tester who wore our designed hybridized self-charging power textile attached to a T-shirt, which harvests light energy and motion energy based on the tester's daily outdoor and indoor activities, respectively. It is also worth noting that the DSSC can efficiently generate electric power under weak light (*42*). The equivalent circuit of the hybridized self-charging power textile is shown in Fig. 5D. A bridge rectifier is used to convert the generated current of F-TENG from ac to direct current before charging the F-SC, a diode is used to block the current of F-TENG that goes through an F-DSSC, and all the switches are used to control the circuit. Although the rectifier, diode, and switches are not flexible, it is possible to design them into either a logo or a button, considering their small size. To simply demonstrate the performance of the as-prepared hybridized self-charging power textile, we design the textile structure in a

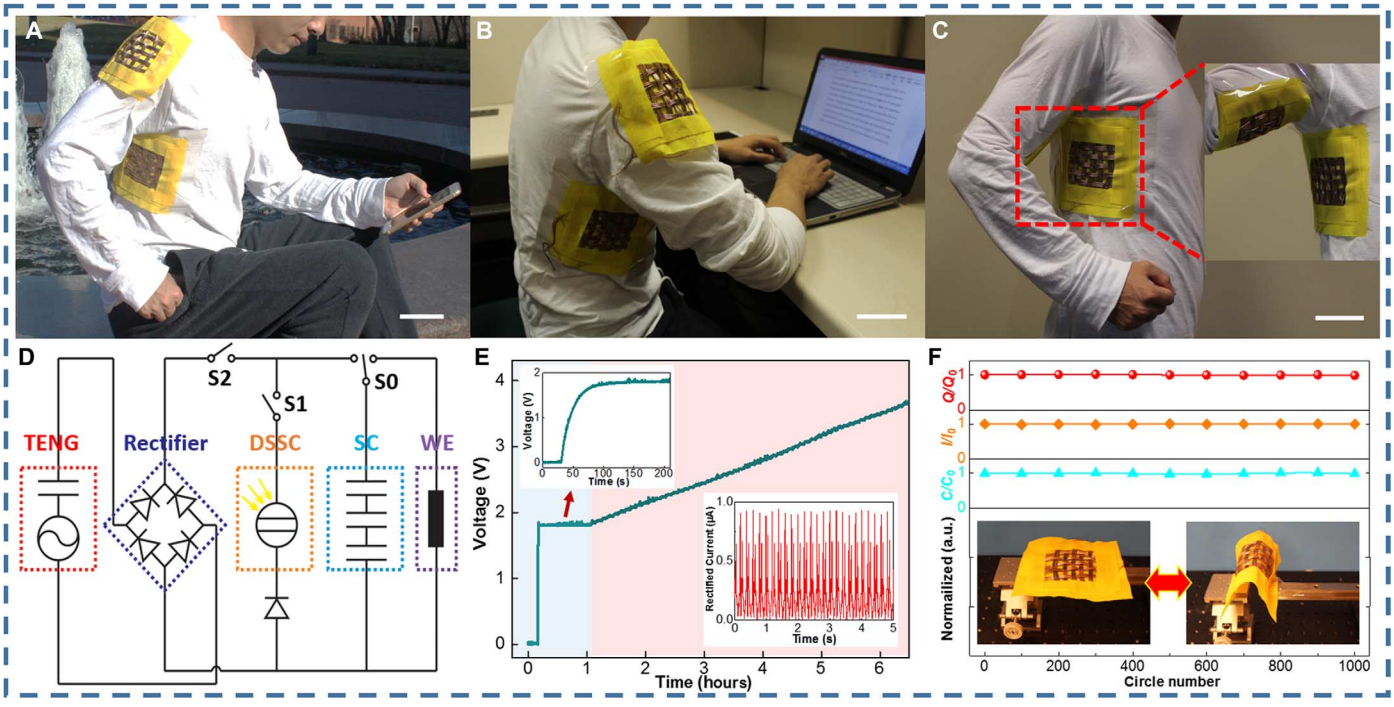

Fig. 5. Demonstration of the self-charging powered textile and its operation under outdoor and indoor conditions. Photograph of the self-charging power textile woven with F-TENGs, F-DSSCs, and F-SCs under outdoor (**A**), indoor (**B**), and movement (**C**) conditions. (**D**) Circuit diagram of the self-charging powered textile for wearable electronics (WE). (**E**) Charging curve of the F-DSSC and the F-TENG, where the light blue–shaded area corresponds to the charging curve of the F-DSSC and the light red–shaded area corresponds to the charging curve of the F-DSSC–F-TENG hybrid. The top left corner inset shows an enlarged curve during the F-DSSC charging period, and the bottom right corner inset shows the rectified I_{SC} of F-TENGs. (**F**) Normalized Q_{SC} values of F-TENGs, I_{SC} values of F-DSSCs, and capacitances of F-SCs bent between 0° and 180° for 1000 cycles. Insets show the photographs of the two final bending statuses (both scale bars, 1 cm). a.u., arbitrary units.

3 × 3 network, meaning that each fabric was connected to three individual F-DSSC or six F-SC units in series and then woven separately. Figure 5E shows the characteristics of the self-charging behavior by harvesting solar and mechanical contact-separation motion energies via the as-prepared hybridized self-charging power textile. Turning the switch S0 on to connect the F-SC to the circuit, while switch S1 is on and switch S2 is off, will linearly increase the voltage of the F-SC (which takes about 69 s to charge from 0 to 1.8 V), indicating the stable output of F-DSSCs. The top left corner inset in Fig. 5E shows the enlarged curve during the charging period of the F-DSSCs. The *I-V* curve of three F-DSSCs with in-series connection is shown in fig. S8. However, the F-SCs remained at 1.8 V because the low output voltage of the F-DSSCs limits their reliability and practicability, as shown in the light blue–shaded area. One effective method to solving this problem is to mimic the in-series structure of F-SCs for electrocytes in the electric eel to produce high working voltages, as reported by Sun *et al.* (*43*). Here, we introduced the TENG with a high voltage output to directly charge the electrochemical capacitors to a high level, which compensates for the weakness of the DSSC. After turning the switch S2 on, the F-SCs can be charged continuously by the F-TENGs to a higher voltage. The corresponding charging curve is plotted in the light red–shaded area. The bottom right corner inset in Fig. 5E shows the rectified I_{SC} of three-series F-TENGs. It should be noted that further improvement in the charging efficiencies can be achieved by obtaining impedance matching among DSSCs, TENGs, and SCs, because the internal impedance of TENGs is generally several orders of magnitude higher than that of DSSCs and SCs. Traditional electronic devices, such as LEDs, digital watches, and a variety of sensors for temperature, pressure, or medical diagnosis, can be easily powered. We believe that, after large-scale fabrication and further improvement, high-power electronic devices—for example, smart bracelets and portable MP3 players—could be charged by our novel self-powered textile in the near future. Last, the durability of the hybridized self-charging power textile was examined under continuous bending motion for 1000 cycles by the linear motor, as shown in Fig. 5F and movie S2. Normalized Q_{SC} values of F-TENGs, I_{SC} values of F-DSSCs, and capacitances of F-SCs were recorded after every 100 times of bending. The insets also display photographs of the textile bent from 0° to 180°. As shown in Fig. 5F, on the basis of their performance, each device showed no significant degradation in performance, confirming their excellent flexibility and stability. The increasing demand for lightweight, highly flexible, stretchable, and washable power modules is one of the critical challenges for the progress of self-powered wearable textiles.

CONCLUSION

In summary, we demonstrate the concept of a hybridized self-charging power textile system with the aim of simultaneously collecting outdoor sunshine and random body motion energies and then transferring them to an energy-storing cell to sustainably operate mobile or wearable electronics. For a single F-DSSC unit, a V_{OC} of 0.74 V and a J_{SC} of 11.92 mA cm^{-2} were achieved, corresponding to an overall power conversion efficiency of 5.64%. The F-TENG can take advantage of human motions, such as jogging, to deliver an output current of up to 0.91 μA. The F-SC unit with the excellent pseudocapacitance of the as-synthesized $RuO_2{\cdot}xH_2O$ exhibits a promising specific capacitance (1.9 mF cm^{-1}), which makes it an effective and flexible electronic energy storage device. Because of the all–fiber-based shape in each device, our proposed hybridized self-charging textile system can be easily woven into electronic textiles to fabricate smart clothes to operate wearable electronic devices. This work presents a welcome advancement for self-powered systems in wearable technology, which will initiate promising improvements in self-powered flexible displays and wearable electronics, among others. A more complicated design is possible because all of the textiles started from 1D building blocks.

MATERIALS AND METHODS

Materials

Lithium iodide (LiI), iodine (I_2), sodium hydroxide (NaOH), ethanol (EtOH), 4-*tert*-butylpyridine (tBP), *tert*-butyl alcohol (tBA), ammonium fluoride (NH_4F), hexachloroplatinic(IV) acid hexahydrate ($H_2PtCl_6{\cdot}6H_2O$), ruthenium(III) chloride ($RuCl_3$), PVA (M_w = 89,000 to 98,000), phosphoric acid solution (H_3PO_4), 3-methoxypropionitrile (MPN), acetonitrile (ACN), titanium tetrachloride ($TiCl_4$), ethylene glycol (EG), 1,2-dimethyl-3-propylimidazolium iodide (DMPII), and *cis*-diisothiocyanato-bis(2,2′-bipyridyl-4,4′-dicarboxylato)ruthenium(II) bis(tetra-butylammonium) (N719 dye) were obtained from Sigma-Aldrich. All chemicals were used as received without further treatment. Miniature clear EVA tubing (length, 10 cm; inside diameter, 0.04″; outer diameter, 0.07″; wall thickness, 0.015″) was purchased from McMaster-Carr. Ti wires (diameter, 0.02″; purity, ~99.99%) and PDMS (Sylgard 184 silicone elastomer) were purchased from Alfa Aesar and Dow Corning, respectively.

Fabrication of the energy-harvesting F-DSSC

Ti wires were polished to remove residual metal oxides and then sequentially cleaned with a neutral cleaner, deionized water, and acetone. A highly ordered TiO_2 nanotube was fabricated on the Ti wire surface by anodization in 0.3 wt % NH_4F/EG solution containing 8 wt % H_2O at a voltage of 60 V via a two-electrode electrochemical cell with a Pt wire as a CE for 6 hours (*44*). After rinsing the surface of the anodized Ti wire with deionized water, the as-prepared Ti wires were gradually annealed to a temperature of 500°C for 1 hour. Afterward, the annealed Ti wires were immersed in 40 mM $TiCl_4$ solution at 70°C for 30 min and then annealed again at 450°C for 30 min. After cooling to 80°C, the annealed Ti wires were immersed in a 3×10^{-4} M solution of N719 dye in ACN and tBA (v/v = 1/1) at room temperature for 24 hours. To fabricate the fiber-based CE, we soaked carbon fiber in an $H_2PtCl_6{\cdot}6H_2O$ aqueous solution (5 mg/ml) for 5 min and then thermally decomposed it at 400°C for 30 min to obtain the Pt-coated carbon fiber, which is used as a CE. To obtain the F-DSSC, we simultaneously inserted a Pt-coated carbon fiber and a dye-sensitized Ti wire into the Cu-coated EVA tubing in parallel and we injected a nonvolatile I^-/I_3^--based electrolyte (0.1 M LiI, 0.05 M I_2, 0.6 M DMPII, and 0.5 M tBP in MPN) into the tubing. Finally, the ends of the tubing were sealed with sealing glue to prevent leakage of the electrolyte.

The solar–to–electrical energy conversion efficiency (η) for a solar cell is given by the J_{SC}, the V_{OC}, and the FF of the cell, and the intensity of the incident light (P_{in}), as shown in Eq. 1

$$\eta = \frac{J_{SC} \times V_{OC} \times FF}{P_{in}} \quad (1)$$

FF can be defined by the ratio of the maximum power (P_{max}) of the solar cell per unit area divided by the V_{OC} and J_{SC}, as shown in Eq. 2

$$FF = \frac{P_{max}}{J_{SC} \times V_{OC}} \quad (2)$$

where P_{max} is obtained as the product of the photocurrent and photovoltage, with the power output of the cell being maximal.

Fabrication of the energy-storing F-SC

A bunch of carbon fibers were ultrasonically cleaned in a mixed solution of acetone, EtOH, and deionized water for 10 min and then coated with $RuCl_3$ slurry made from 0.1 g of $RuCl_3$ and 4 ml of EtOH. After drying at 60°C, the carbon fibers were fixed on a shelf and then placed in a 50-ml Teflon-lined stainless steel autoclave with 1 ml of 0.1 M NaOH solution. The autoclave was kept in an oven at 190°C for 5 hours and then cooled down to room temperature in air. After washing and drying, $RuO_2{\cdot}xH_2O$–coated carbon fibers were obtained. The PVA/H_3PO_4 gel electrolyte was prepared by adding 5 g of H_3PO_4 and 5 g of PVA powder into 50 ml of deionized water. The mixture was heated to 85°C under stirring until the solution became clear. The as-prepared $RuO_2{\cdot}xH_2O$–coated carbon fibers were immersed into PVA/H_3PO_4 solution for 10 min, with their two-end parts kept above the solution. After being taken out, two fibers were assembled into PDMS-covered Cu-coated tubing, separated by a paper septum and leaving aside the bare part as the electrode terminal.

The length-specific capacitance and energy density can be calculated from the GCD curve by using Eqs. 3 and 4, respectively

$$C = \frac{I \times \Delta t}{\Delta V \times l} \quad (3)$$

$$E = {}^1\!/_2 C \times \Delta V^2 \quad (4)$$

where C is the length-specific capacitance of F-SC, I is the constant current, Δt is the discharge time, ΔV is the voltage change during the discharge process, l is the total length for both carbon electrodes, and E is the energy density.

Fabrication of the energy-harvesting F-TENG

Commercial miniature clear EVA tubing was used to fabricate the F-TENG. The tubing was cleaned with isopropanol and then washed with abundant deionized water by ultrasonic cleaning. After drying, a copper lead wire was attached to the tubing with conductive adhesive epoxy. Subsequently, a layer of copper electrode was deposited onto one side of the EVA tubing surface by physical vapor deposition with a power of 100 W under Ar atmosphere for 40 min (layer thickness, 1 μm). Afterward, the PDMS elastomer and the curing agent were mixed (w/w = 10/1) and then coated on the surface of the as-prepared Cu-coated EVA tubing through a "dipping and drying" process (*45*, *46*). After drying at room temperature for 12 hours, PDMS-covered Cu-coated EVA tubing was obtained. A single F-TENG unit can be assembled by connecting Cu-coated EVA tubing as a triboelectric electrode and PDMS-covered Cu-coated EVA tubing as another electrode.

Fabrication of the hybridized self-charging power textile

First, the as-prepared F-DSSCs and F-SCs could be easily woven as the textile with different net structures, as shown in Fig. 1. The output voltage and capacitance of the as-woven textile could be easily tuned by in-series and/or parallel connection to drive real wearable electronics. To fabricate the hybridized self-charging power textile, the woven F-DSSC textile was used as the top layer to harvest sunlight energy, and the woven F-SC textile was used as the bottom layer to store harvested energies. Meanwhile, both woven textiles simultaneously played as triboelectric layers to gather mechanical energies from human motion, which were then also collected via the woven F-SC textile after rectification.

Characterization and measurement

Field-emission SEM (Hitachi SU8010) was used to measure the morphology and size of the TiO_2 nanotube arrays on the Ti wire and $RuO_2{\cdot}xH_2O$–coated carbon fibers. The crystal phase identification of both the as-prepared TiO_2 nanotube and $RuO_2{\cdot}xH_2O$ was investigated by the XRD system (Bede D1) with Cu-Kα1 radiation (λ = 0.15406 nm). For the electric output measurement of the F-TENG, a linear motor (Linmot E1100) was applied to mimic human motions, driving the TENG contact-separation process. A programmable electrometer (Keithley 6514) was adopted to test the V_{OC}, I_{SC}, and Q_{SC}. The software platform was constructed on the basis of LabVIEW, which is capable of realizing real-time data acquisition control and analysis. The *J-V* characteristic of the F-DSSC was recorded by a Keithley 2400 electrometer under illumination (100 mW/cm^2) of simulated solar light (Oriel 91160-1000 equipped with a 450-W Xe lamp; AM1.5). The light intensity was calibrated using a reference Si solar cell (Oriel 70260). The effective area of the F-DSSC was defined by multiplying the length by the diameter of the photoanode. The F-DSSC body remained vertical with the light, whether straight or bending. The electrochemical performance of the F-SC was measured by an electrochemical workstation (Princeton Applied Research VersaSTAT 3). A potentiostat was used to test capacitance properties with CV and GCD techniques. The charging/discharging process of the self-charging power system was tested with a battery analyzer.

SUPPLEMENTARY MATERIALS

Supplementary material for this article is available at http://advances.sciencemag.org/cgi/content/full/2/10/e1600097/DC1

fig. S1. XRD pattern of the anodized TiO_2 nanotube arrays on a Ti wire.
fig. S2. SEM images of the pure carbon fiber and the Pt-coated carbon fiber.
fig. S3. *J-V* curve of an F-DSSC based on bare carbon fibers.
fig. S4. Dependence of an F-DSSC at different incident light angles.
fig. S5. XRD pattern of the $RuO_2{\cdot}xH_2O$.
fig. S6. CV and GCD curves of an F-SC based on bare carbon fibers.
fig. S7. V_{OC} outputs of F-TENG network textiles.
fig. S8. *I-V* curve of three F-DSSCs with in-series connection.
movie S1. Flexibility test of Cu-coated EVA tubing.
movie S2. Stability test of hybridized self-charging power textile.

REFERENCES AND NOTES

1. D. Son, J. Lee, S. Qiao, R. Ghaffari, J. Kim, J. E. Lee, C. Song, S. J. Kim, D. J. Lee, S. W. Jun, S. Yang, M. Park, J. Shin, K. Do, M. Lee, K. Kang, C. S. Hwang, N. Lu, T. Hyeon, D.-H. Kim, Multifunctional wearable devices for diagnosis and therapy of movement disorders. *Nat. Nanotechnol.* **9**, 397–404 (2014).
2. M. J. Cima, Next-generation wearable electronics. *Nat. Biotechnol.* **32**, 642–643 (2014).
3. M. Ha, J. Park, Y. Lee, H. Ko, Triboelectric generators and sensors for self-powered wearable electronics. *ACS Nano* **9**, 3421–3427 (2015).

4. H.-H. Chou, A. Nguyen, A. Chortos, J. W. F. To, C. Lu, J. Mei, T. Kurosawa, W.-G. Bae, J. B.-H. Tok, Z. Bao, A chameleon-inspired stretchable electronic skin with interactive colour changing controlled by tactile sensing. *Nat. Commun.* **6**, 8011 (2015).
5. E. Dolgin, Technology: Dressed to detect. *Nature* **511**, S16–S17 (2014).
6. R. Hinchet, W. Seung, S.-W. Kim, Recent progress on flexible triboelectric nanogenerators for selfpowered electronics. *ChemSusChem* **8**, 2327–2344 (2015).
7. J. Deng, Y. Zhang, Y. Zhao, P. Chen, X. Cheng, H. Peng, A shape-memory supercapacitor fiber. *Angew. Chem. Int. Ed.* **54**, 15419–15429 (2015).
8. J. Bae, M. K. Song, Y. J. Park, J. M. Kim, M. Liu, Z. L. Wang, Fiber supercapacitors made of nanowire-fiber hybrid structures for wearable/flexible energy storage. *Angew. Chem. Int. Ed.* **50**, 1683–1687 (2011).
9. T. Chen, L. Qiu, Z. Yang, Z. Cai, J. Ren, H. Li, H. Lin, X. Sun, H. Peng, An integrated "energy wire" for both photoelectric conversion and energy storage. *Angew. Chem. Int. Ed.* **51**, 11977–11980 (2012).
10. Z. Zhang, X. Chen, P. Chen, G. Guan, L. Qiu, H. Lin, Z. Yang, W. Bai, Y. Luo, H. Peng, Integrated polymer solar cell and electrochemical supercapacitor in a flexible and stable fiber format. *Adv. Mater.* **26**, 466–470 (2014).
11. Y. Fu, H. Wu, S. Ye, X. Cai, X. Yu, S. Hou, H. Kafafy, D. Zou, Integrated power fiber for energy conversion and storage. *Energy Environ. Sci.* **6**, 805–812 (2013).
12. P. Du, X. Hu, C. Yi, H. C. Liu, P. Liu, H.-L. Zhang, X. Gong, Self-powered electronics by integration of flexible solid-state graphene-based supercapacitors with high performance perovskite hybrid solar cells. *Adv. Funct. Mater.* **25**, 2420–2427 (2015).
13. C. Xu, Z. L. Wang, Compact hybrid cell based on a convoluted nanowire structure for harvesting solar and mechanical energy. *Adv. Mater.* **23**, 873–877 (2011).
14. C. Xu, X. Wang, Z. L. Wang, Nanowire structured hybrid cell for concurrently scavenging solar and mechanical energies. *J. Am. Chem. Soc.* **131**, 5866–5872 (2009).
15. C. Xu, C. Pan, Y. Liu, Z. L. Wang, Hybrid cells for simultaneously harvesting multi-type energies for self-powered micro/nanosystems. *Nano Energy* **1**, 259–272 (2012).
16. Y. Yang, H. Zhang, G. Zhu, S. Lee, Z.-H. Lin, Z. L. Wang, Flexible hybrid energy cell for simultaneously harvesting thermal, mechanical, and solar energies. *ACS Nano* **7**, 785–790 (2013).
17. Y. Yang, Z. L. Wang, Hybrid energy cells for simultaneously harvesting multi-types of energies. *Nano Energy* **14**, 245–256 (2015).
18. Q. Liang, X. Yan, Y. Gu, K. Zhang, M. Liang, S. Lu, X. Zheng, Y. Zhang, Highly transparent triboelectric nanogenerator for harvesting water-related energy reinforced by antireflection coating. *Sci. Rep.* **5**, 9080 (2015).
19. Z. L. Wang, J. Chen, L. Lin, Progress in triboelectric nanogenerators as a new energy technology and self-powered sensors. *Energy Environ. Sci.* **8**, 2250–2282 (2015).
20. Y. Zi, S. Niu, J. Wang, Z. Wen, W. Tang, Z. L. Wang, Standards and figure-of-merits for quantifying the performance of triboelectric nanogenerators. *Nat. Commun.* **6**, 8376 (2015).
21. J. Chen, J. Yang, Z. Li, X. Fan, Y. Zi, Q. Jing, H. Guo, Z. Wen, K. C. Pradel, S. Niu, Z. L. Wang, Networks of triboelectric nanogenerators for harvesting water wave energy: A potential approach toward blue energy. *ACS Nano* **9**, 3324–3331 (2015).
22. R. Zhang, S. Wang, M.-H. Yeh, C. Pan, L. Lin, R. Yu, Y. Zhang, L. Zheng, Z. Jiao, Z. L. Wang, A streaming potential/current-based microfluidic direct current generator for self-powered nanosystems. *Adv. Mater.* **27**, 6482–6487 (2015).
23. Q. Liang, X. Yan, X. Liao, S. Cao, X. Zheng, H. Si, S. Lu, Y. Zhang, Multi-unit hydroelectric generator based on contact electrification and its service behavior. *Nano Energy* **16**, 329–338 (2015).
24. H. Guo, Z. Wen, Y. Zi, M.-H. Yeh, J. Wang, L. Zhu, C. Hu, Z. L. Wang, A water-proof triboelectric–electromagnetic hybrid generator for energy harvesting in harsh environments. *Adv. Energy Mater.* **6**, 1501593 (2015).
25. Z. Wen, J. Chen, M.-H. Yeh, H. Guo, Z. Li, X. Fan, T. Zhang, L. Zhu, Z. L. Wang, Blow-driven triboelectric nanogenerator as an active alcohol breath analyzer. *Nano Energy* **16**, 38–46 (2015).
26. M.-H. Yeh, H. Guo, L. Lin, Z. Wen, Z. Li, C. Hu, Z. L. Wang, Rolling friction enhanced free-standing triboelectric nanogenerators and their applications in self-powered electrochemical recovery systems. *Adv. Funct. Mater.* **26**, 1054–1062 (2015).
27. Z. Wen, H. Guo, Y. Zi, M.-H. Yeh, X. Wang, J. Deng, J. Wang, S. Li, C. Hu, L. Zhu, Z. L. Wang, Harvesting broad frequency band blue energy by a triboelectric–electromagnetic hybrid nanogenerator. *ACS Nano* **10**, 6526–6534 (2016).
28. Z. Li, J. Chen, J. Yang, Y. Su, X. Fan, Y. Wu, C. Yu, Z. L. Wang, β-Cyclodextrin enhanced triboelectrification for self-powered phenol detection and electrochemical degradation. *Energy Environ. Sci.* **8**, 887–896 (2015).
29. X. Pu, L. Li, H. Song, C. Du, Z. Zhao, C. Jiang, G. Cao, W. Hu, Z. L. Wang, A self-charging power unit by integration of a textile triboelectric nanogenerator and a flexible lithium-ion battery for wearable electronics. *Adv. Mater.* **27**, 2472–2478 (2015).
30. W. Seung, M. K. Gupta, K. Y. Lee, K.-S. Shin, J.-H. Lee, T. Y. Kim, S. Kim, J. Lin, J. H. Kim, S.-W. Kim, Nanopatterned textile-based wearable triboelectric nanogenerator. *ACS Nano* **9**, 3501–3509 (2015).
31. C. Pan, W. Guo, L. Dong, G. Zhu, Z. L. Wang, Optical fiber-based core–shell coaxially structured hybrid cells for self-powered nanosystems. *Adv. Mater.* **24**, 3356–3361 (2012).
32. H. Guo, X. He, J. Zhong, Q. Zhong, Q. Leng, C. Hu, J. Chen, L. Tian, Y. Xi, J. Zhou, A nanogenerator for harvesting airflow energy and light energy. *J. Mater. Chem. A* **2**, 2079–2087 (2014).
33. Y. Zi, L. Lin, J. Wang, S. Wang, J. Chen, X. Fan, P.-K. Yang, F. Yi, Z. L. Wang, Triboelectric–pyroelectric–piezoelectric hybrid cell for high-efficiency energy-harvesting and self-powered sensing. *Adv. Mater.* **27**, 2340–2347 (2015).
34. J. Wang, X. Li, Y. Zi, S. Wang, Z. Li, L. Zheng, F. Yi, S. Li, Z. L. Wang, A flexible fiber-based supercapacitor–triboelectric-nanogenerator power system for wearable electronics. *Adv. Mater.* **27**, 4830–4836 (2015).
35. S. Pan, Z. Yang, P. Chen, X. Fang, G. Guan, Z. Zhang, J. Deng, H. Peng, Carbon nanostructured fibers as counter electrodes in wire-shaped dye-sensitized solar cells. *J. Phys. Chem. C* **118**, 16419–16425 (2014).
36. J. Park, J. W. Lee, B. U. Ye, S. H. Chun, S. H. Joo, H. Park, H. Lee, H. Y. Jeong, M. H. Kim, J. M. Baik, Structural evolution of chemically-driven RuO_2 nanowires and 3-dimensional design for photo-catalytic applications. *Sci. Rep.* **5**, 11933 (2015).
37. Z.-S. Wu, D.-W. Wang, W. Ren, J. Zhao, G. Zhou, F. Li, H.-M. Cheng, Anchoring hydrous RuO_2 on graphene sheets for high-performance electrochemical capacitors. *Adv. Funct. Mater.* **20**, 3595–3602 (2010).
38. X. Fan, J. Chen, J. Yang, P. Bai, Z. Li, Z. L. Wang, Ultrathin, rollable, paper-based triboelectric nanogenerator for acoustic energy harvesting and self-powered sound recording. *ACS Nano* **9**, 4236–4243 (2015).
39. S. Li, S. Wang, Y. Zi, Z. Wen, L. Lin, G. Zhang, Z. L. Wang, Largely improving the robustness and lifetime of triboelectric nanogenerators through automatic transition between contact and noncontact working states. *ACS Nano* **9**, 7479–7487 (2015).
40. J. Chen, J. Yang, H. Guo, Z. Li, L. Zheng, Y. Su, Z. Wen, X. Fan, Z. L. Wang, Automatic mode transition enabled robust triboelectric nanogenerators. *ACS Nano* **9**, 12334–12343 (2015).
41. X. Li, M.-H. Yeh, Z.-H. Lin, H. Guo, P.-K. Yang, J. Wang, S. Wang, R. Yu, T. Zhang, Z. L. Wang, Self-powered triboelectric nanosensor for microfluidics and cavity-confined solution chemistry. *ACS Nano* **9**, 11056–11063 (2015).
42. G. Liu, M. Peng, W. Song, H. Wang, D. Zou, An 8.07% efficient fiber dye-sensitized solar cell based on a TiO_2 micron-core array and multilayer structure photoanode. *Nano Energy* **11**, 341–347 (2015).
43. H. Sun, X. Fu, S. Xie, Y. Jiang, H. Peng, Electrochemical capacitors with high output voltages that mimic electric eels. *Adv. Mater.* **28**, 2070–2076 (2016).
44. Z. Yang, J. Deng, X. Sun, H. Li, H. Peng, Stretchable, wearable dye-sensitized solar cells. *Adv. Mater.* **26**, 2643–2647 (2014).
45. J. Zhong, Y. Zhang, Q. Zhong, Q. Hu, B. Hu, Z. L. Wang, J. Zhou, Fiber-based generator for wearable electronics and mobile medication. *ACS Nano* **8**, 6273–6280 (2014).
46. J. Zhong, Q. Zhong, Q. Hu, N. Wu, W. Li, B. Wang, B. Hu, J. Zhou, Stretchable self-powered fiber-based strain sensor. *Adv. Funct. Mater.* **25**, 1798–1803 (2015).

Acknowledgments

Funding: Research was supported by the Hightower Chair Foundation, the National Key R&D Project from the Ministry of Science and Technology (2016YFA0202704), and the "Thousands Talents" program for pioneer researcher and his innovation team of China. Z.W. thanks the China Scholarship Council for supporting research at the Georgia Institute of Technology, USA. **Author contributions:** Z.W., M.-H.Y., and Z.L.W. conceived the idea. Z.W., M.-H.Y., and H.G. designed the experiments. Z.W., M.-H.Y., H.G., and J.W. performed the F-SC experiments. M.-H.Y., H.G., W.X., L.Z., X.W., and X.S. performed the F-DSSC experiments. Z.W., H.G., and J.D. performed the F-TENG experiments. Z.W., M.-H.Y., H.G., Y.Z., C.H., and L.Z. graphed and analyzed the data. Z.W., M.-H.Y., and Z.L.W. wrote the paper. All authors discussed the results and commented on the manuscript. **Competing interests:** The authors declare that they have no competing interests. **Data and materials availability:** All data needed to evaluate the conclusions in the paper are present in the paper and/or the Supplementary Materials. Additional data related to this paper may be requested from the authors.

Submitted 19 January 2016
Accepted 26 September 2016
Published 26 October 2016
10.1126/sciadv.1600097

Citation: Z. Wen, M.-H. Yeh, H. Guo, J. Wang, Y. Zi, W. Xu, J. Deng, L. Zhu, X. Wang, C. Hu, L. Zhu, X. Sun, Z. L. Wang, Self-powered textile for wearable electronics by hybridizing fiber-shaped nanogenerators, solar cells, and supercapacitors. *Sci. Adv.* **2**, e1600097 (2016).

ScienceAdvances
AAAS

Self-powered textile for wearable electronics by hybridizing fiber-shaped nanogenerators, solar cells, and supercapacitors

Zhen Wen, Min-Hsin Yeh, Hengyu Guo, Jie Wang, Yunlong Zi, Weidong Xu, Jianan Deng, Lei Zhu, Xin Wang, Chenguo Hu, Liping Zhu, Xuhui Sun and Zhong Lin Wang (October 26, 2016)
Sci Adv 2016, 2:.
doi: 10.1126/sciadv.1600097